JOURNAL OF MATERIALS SCIENCE 13 (1978) 473–482

The incorporation of ambipolar diffusion in deformation mechanism maps for ceramics

TERENCE G. LANGDON, FARGHALLI A. MOHAMED
Department of Materials Science, University of Southern California, Los Angeles, California 90007, USA

Ambipolar diffusion gives rise to four distinct types of diffusion creep in ceramic materials, depending on whether the processes of lattice and grain-boundary diffusion creep are controlled by the anions or cations, respectively. These four processes are incorporated in a deformation mechanism map for diffusion creep in pure Al_2O_3, using a new form of map which is independent of the selected stress level. This map may be used to determine the rate-controlling mechanism for diffusion creep under any selected experimental conditions. By superimposing dislocation creep on to the map, it is possible to estimate the highest permissible stress and the lowest feasible temperature for experimental observation of any of the diffusion creep processes.

1. Introduction

Since the work of Ashby [1] on the development of deformation mechanism maps for a number of different materials, deformation mapping has become firmly established as an important tool in the representation of mechanical data. The rapid acceptance of this technique may be readily illustrated by noting that examples of maps are included in several very recent introductory [2–4] and advanced [5–8] texts.

Two basic types of deformation mechanism map have been developed to date. The first type, originally suggested by Weertman and Weertman [9, 10], plots normalized stress against homologous temperature at constant grain size. The second type, suggested by Mohamed and Langdon [11], plots normalized grain size against normalized stress at constant temperature.

Maps of both types have been presented for several different ceramic materials. For the first type, maps are now available for CoO [12–14], $MgAl_2O_4$ [13], olivine $[(Mg_{0.85}Fe_{0.15})_2SiO_4-(Mg_{0.95}Fe_{0.05})_2SiO_4]$ [15–17], MgO [1, 15], NiO [18], PbS [19], SiC [20], UC [21], UO_2 [1, 22], and $ZrC_{0.95}$ [23]; for the second type, maps are available for Al_2O_3, KCl, LiF, MgO, NaCl, and UC [24].

When constructing deformation mechanism maps, the procedure adopted is to estimate the best constitutive equations for the various deformation processes, and then to plot these relationships in terms of two of the permissible variables. To date, all of the maps developed for ceramic materials have considered two distinct types of stress-directed diffusional creep: Nabarro–Herring creep [25, 26], where vacancies diffuse through the lattice, and Coble creep [27], where vacancies diffuse along the grain boundaries. In every case, it has been assumed that the anions and cations move together along the same path, and the diffusional process is controlled by the movement of the slower diffusing ion. In practice, however, ambipolar diffusion may take place in an ionic compound, so that there is simultaneous mass transport of the anions and cations along parallel, but different, diffusion paths. Under steady-state conditions, the total flow associated with each ionic component remains in the stoichiometric ratio as a result of ambipolar diffusion, but the

net current flow along each parallel diffusion path is not necessarily zero.

It has been established that ambipolar diffusion plays an important role in the creep of ceramic materials [28–30]. The purpose of this paper is therefore two-fold. First, to investigate the effect of incorporating ambipolar diffusion in deformation mechanism maps for ceramics. Second, to demonstrate a new form of map, introduced elsewhere [31], which is particularly suited for ceramic materials when ambipolar diffusion is included.

2. Diffusion creep in ceramics

When creep occurs by the Nabarro–Herring process, the steady-state creep rate is given by

$$\dot{\epsilon}_N = A_N \left(\frac{\Omega_v}{b^3}\right)\left(\frac{Gb}{kT}\right)\left(\frac{b}{d}\right)^2\left(\frac{\sigma}{G}\right)D_l \quad (1)$$

where A_N is a dimensionless constant ($\simeq 40$), Ω_v is the molecular volume, b is the Burgers vector, G is the shear modulus, k is Boltzmann's constant, T is the absolute temperature, d is the grain size, σ is the applied stress, and D_l is the coefficient for lattice diffusion.

When creep occurs by the Coble process, the steady-state creep rate is given by

$$\dot{\epsilon}_{Co} = A_{Co}\left(\frac{\Omega_v}{b^3}\right)\left(\frac{Gb}{kT}\right)\left(\frac{b}{d}\right)^2\left(\frac{\sigma}{G}\right)\left(\frac{\delta D_{gb}}{d}\right) \quad (2)$$

where A_{Co} is a dimensionless constant ($\simeq 150/\pi$), δ is the effective width of the grain boundary for enhanced diffusion, and D_{gb} is the grain boundary diffusion coefficient.

For monatomic materials, the vacancies may diffuse along either path and the total strain rate due to diffusional creep, $\dot{\epsilon}_{dc}$, is equal to the sum of the individual rates due to lattice and grain-boundary diffusion:

$$\dot{\epsilon}_{dc} = \dot{\epsilon}_N + \dot{\epsilon}_{Co} \quad (3)$$

However, in an ionic compound of the type $A_\alpha B_\beta$, in which the valence of the cation A is $\beta+$ and the valence of the anion B is $\alpha-$, both the cations and the anions participate in the diffusion process, and these two atomic species may diffuse along different paths [28]. In this case, the total strain rate is given by [32]

$$\dot{\epsilon}_{dc} = A_{dc}\left(\frac{\Omega_v}{b^3}\right)\left(\frac{Gb}{kT}\right)\left(\frac{b}{d}\right)^2\left(\frac{\sigma}{G}\right)D_{complex} \quad (4)$$

where A_{dc} is a dimensionless constant ($\simeq 40$), and $D_{complex}$ is defined as

$$D_{complex} = \frac{(1/\alpha)\,[D_l^+ + 1.2(\delta^+ D_{gb}^+/d)]}{1 + (\beta/\alpha)\dfrac{[D_l^+ + 1.2(\delta^+ D_{gb}^+/d)]}{[D_l^- + 1.2(\delta^- D_{gb}^-/d)]}} \quad (5)$$

where D_l^+, D_{gb}^+, and δ^+ are the lattice diffusivity, grain boundary diffusivity, and effective grain boundary width, respectively, for the $A^{\beta+}$ cation, and D_l^-, D_{gb}^-, and δ^- are the same terms for the $B^{\alpha-}$ anion.

Depending on the relative magnitudes of the lattice and grain-boundary diffusivities for the A and B ions, Equation 4 shows that there are four possible types of diffusion creep in ionic compounds: Nabarro–Herring creep controlled by diffusion of either the cation ($\dot{\epsilon}_N^+$) or anion ($\dot{\epsilon}_N^-$), and Coble creep controlled by diffusion of either the cation ($\dot{\epsilon}_{Co}^+$) or anion ($\dot{\epsilon}_{Co}^-$). The equations for these processes are shown in Table I,

TABLE I Types of diffusion creep in ceramics

Type	Equation	Number
Cation-controlled Nabarro–Herring creep	$\dot{\epsilon}_N^+ = \left(\frac{A_{dc}}{\alpha}\right)\left(\frac{\Omega_v}{b^3}\right)\left(\frac{Gb}{kT}\right)\left(\frac{b}{d}\right)^2\left(\frac{\sigma}{G}\right)D_l^+$	(6)
Anion-controlled Nabarro–Herring creep	$\dot{\epsilon}_N^- = \left(\frac{A_{dc}}{\beta}\right)\left(\frac{\Omega_v}{b^3}\right)\left(\frac{Gb}{kT}\right)\left(\frac{b}{d}\right)^2\left(\frac{\sigma}{G}\right)D_l^-$	(7)
Cation-controlled Coble creep	$\dot{\epsilon}_{Co}^+ = \left(\frac{1.2A_{dc}}{\alpha}\right)\left(\frac{\Omega_v}{b^3}\right)\left(\frac{Gb}{kT}\right)\left(\frac{b}{d}\right)^2\left(\frac{\sigma}{G}\right)\left(\frac{\delta^+ D_{gb}^+}{d}\right)$	(8)
Anion-controlled Coble creep	$\dot{\epsilon}_{Co}^- = \left(\frac{1.2A_{dc}}{\beta}\right)\left(\frac{\Omega_v}{b^3}\right)\left(\frac{Gb}{kT}\right)\left(\frac{b}{d}\right)^2\left(\frac{\sigma}{G}\right)\left(\frac{\delta^- D_{gb}^-}{d}\right)$	(9)

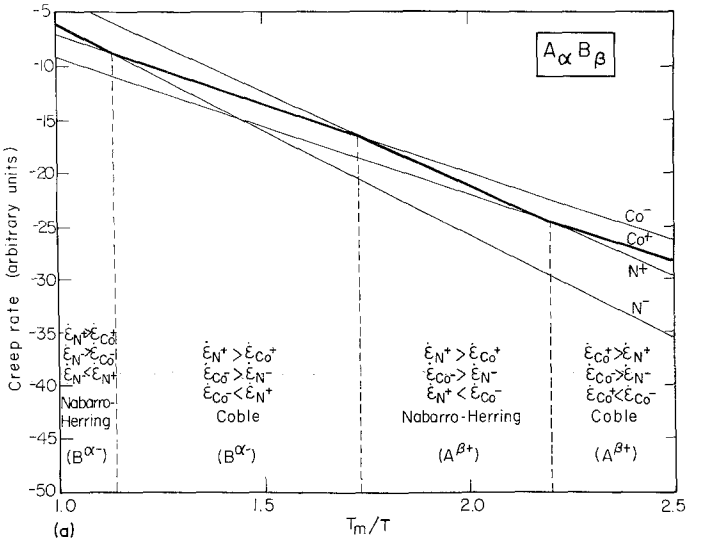

Figure 1 Logarithmic creep rate versus the reciprocal of homologous temperature for a hypothetical compound $A_\alpha B_\beta$, indicating the four diffusion creep processes and the calculations to determine the rate-controlling mechanism. (a) Cations control the behaviour at low temperatures and anions at high temperatures; (b) anions control the behaviour at low temperatures and cations at high temperatures.

representing the four limiting conditions of Equation 4.

The various classes of behaviour arising for different values of grain size and temperature are described in detail elsewhere [32]. Under any experimental conditions, it follows from Equation 4 that the total strain rate experienced by an ionic compound during diffusion creep is determined by the movement of the slower diffusing species along the faster diffusion path.

An examination of Equations 6 to 9 shows that, neglecting the terms $1/\alpha$ and $1/\beta$ for cation and anion control, respectively,* and also the relatively minor difference of a factor of 1.2 in the relationships for Coble creep, the rate-controlling process is determined exclusively by the relative magnitudes of D_l^+, D_l^-, $\delta^+ D_{gb}^+/d$, and $\delta^- D_{gb}^-/d$. Since the two relationships for Coble creep include an inverse dependence on grain size in addition to the standard $(b/d)^2$ term, the rate-controlling process under any experimental conditions depends on both temperature and grain size.

The temperature dependence at constant grain size is illustrated schematically in Fig. 1 for a hypothetical compound $A_\alpha B_\beta$, where the logarithmic creep rate (in arbitrary units) is plotted as a function of the reciprocal of the homologous temperature, T_m/T, from 0.4 to 1.0 T_m, where T_m is the melting point of the material in degrees

*For many ceramic materials, such as BeO, LiF, MgO, and NaCl, Equations 6 to 9 are simplified because $\alpha = \beta = 1$.

Kelvin. The four lines shown in the upper portions of the diagrams represent typical creep rates for $\dot{\epsilon}_N^+$, $\dot{\epsilon}_N^-$, $\dot{\epsilon}_{Co}^+$, and $\dot{\epsilon}_{Co}^-$, respectively*.

Over any selected range of temperature, the rate-controlling mechanism is obtained by a two-step procedure. First, it is necessary to identify the faster process for both the anions and the cations, since this indicates the preferred diffusive paths. Second, it is necessary to determine the slower of these two processes, since this gives the rate-controlling mechanism.

The relevant calculations are shown in the lower portions of Fig. 1, and the rate-controlling process is indicated by the thicker line in the upper portions. For example, at the lowest temperatures in Fig. 1a, Coble creep via the grain boundaries is the faster process for both the cations ($\dot{\epsilon}_{Co}^+ > \dot{\epsilon}_N^+$) and the anions ($\dot{\epsilon}_{Co}^- > \dot{\epsilon}_N^-$). A comparison of the two Coble creep rates shows that $\dot{\epsilon}_{Co}^+ < \dot{\epsilon}_{Co}^-$, so that the rate-controlling process is Coble creep for the $A^{\beta+}$ cation.

For this hypothetical case, Fig. 1a shows four distinct regions of behaviour over the temperature range from 0.4 to 1.0 T_m: cation-controlled Coble creep, cation-controlled Nabarro–Herring creep, anion-controlled Coble creep, and anion-controlled Nabarro–Herring creep. This result is significant because it reveals the possibility of a transition from Nabarro–Herring creep to Coble creep with an increase in temperature at constant grain size. This situation contrasts with monatomic systems where, at constant grain size, the transition is always from Coble creep to Nabarro–Herring creep with increasing temperature. As indicated in Fig. 1a, the transition in ionic compounds is accompanied by a change in the rate-controlling ion.

A similar set of data is shown in Fig. 1b, except that in this case the $B^{\alpha-}$ anion is the rate-controlling species at the lower temperatures. An alternative possibility, not illustrated in Fig. 1a, is a transition from the two Coble processes at the lower temperatures to the two Nabarro–Herring processes at the higher temperatures: for example, Coble ($B^{\alpha-}$) → Coble ($A^{\beta+}$) → Nabarro–Herring ($B^{\alpha-}$) → Nabarro–Herring ($A^{\beta+}$). As will be demonstrated, in a real material for a single grain size, all four mechanisms are not necessarily revealed over the temperature range from 0.4 to 1.0 T_m.

3. Diffusion creep in aluminium oxide

Undoped aluminium oxide was selected for the purpose of illustration, because of the availability of good experimental data for both the lattice and grain boundary diffusivities.

For the cation, the lattice [33] and grain-boundary [34] diffusion coefficients are given by

$$D_l^+ = 28 \exp(-478\,000/RT)\,\mathrm{cm^2\,sec^{-1}} \quad (10)$$

and

$$\delta^+ D_{gb}^+ = 8.6 \times 10^{-4} \exp(-419\,000/RT)\,\mathrm{cm^3\,sec^{-1}} \quad (11)$$

where R is the gas constant (8.31 J mol^{-1} K^{-1}).

For the anion, the lattice diffusion coefficient is given by [35]

$$D_l^- = 1.9 \times 10^3 \exp(-637\,000/RT)\,\mathrm{cm^2\,sec^{-1}} \quad (12)$$

The value of $\delta^- D_{gb}^-$ for the anion was estimated from the line calculated as a lower bound by Cannon and Coble [34] (see their Fig. 8), to give

$$\delta^- D_{gb}^- = 2 \times 10^{-6} \exp(-226\,000/RT)\,\mathrm{cm^3\,sec^{-1}} \quad (13)$$

In addition, $\Omega_v = 4.20 \times 10^{-23}$ cm^3 and $b = 4.75 \times 10^{-8}$ cm for slip on the $\{0\,0\,0\,1\}\langle 1\,1\,\bar{2}\,0\rangle$ basal system in Al_2O_3. Taking $A_{dc} = 40$ in Equations 6 to 9, and using the diffusivities given by Equations 10 to 13, the creep rates in arbitrary units were logarithmically plotted against T_m/T for four grain sizes, each differing by an order of magnitude, from 10 μm to 1 cm†. The results, shown in Fig. 2, are in the same format as Fig. 1, and again indicate the calculations required to determine the rate-controlling process. Fig. 2a shows that cation-controlled Coble creep is the dominant process over the entire temperature range for a grain size of 10 μm; but, as indicated in Fig. 2b, an increase in grain size to 100 μm leads to a transition to cation-controlled Nabarro–Herring

*Since $Q_{gb} < Q_l$, where Q_{gb} and Q_l are the activation energies for grain-boundary and lattice diffusion, respectively, the slopes of the lines for Coble creep in Fig. 1 are necessarily lower than the slopes for Nabarro–Herring creep for the same ion.

†For convenience, the creep rates were expressed in arbitrary units so that the term $(\Omega_v/b^3)(Gb/kT)(b/d)^2(\sigma/G)$, which is common to each equation for diffusion creep, may be excluded. The creep rates shown in Fig.2 were calculated from the first and last terms in Equations 6 to 9.

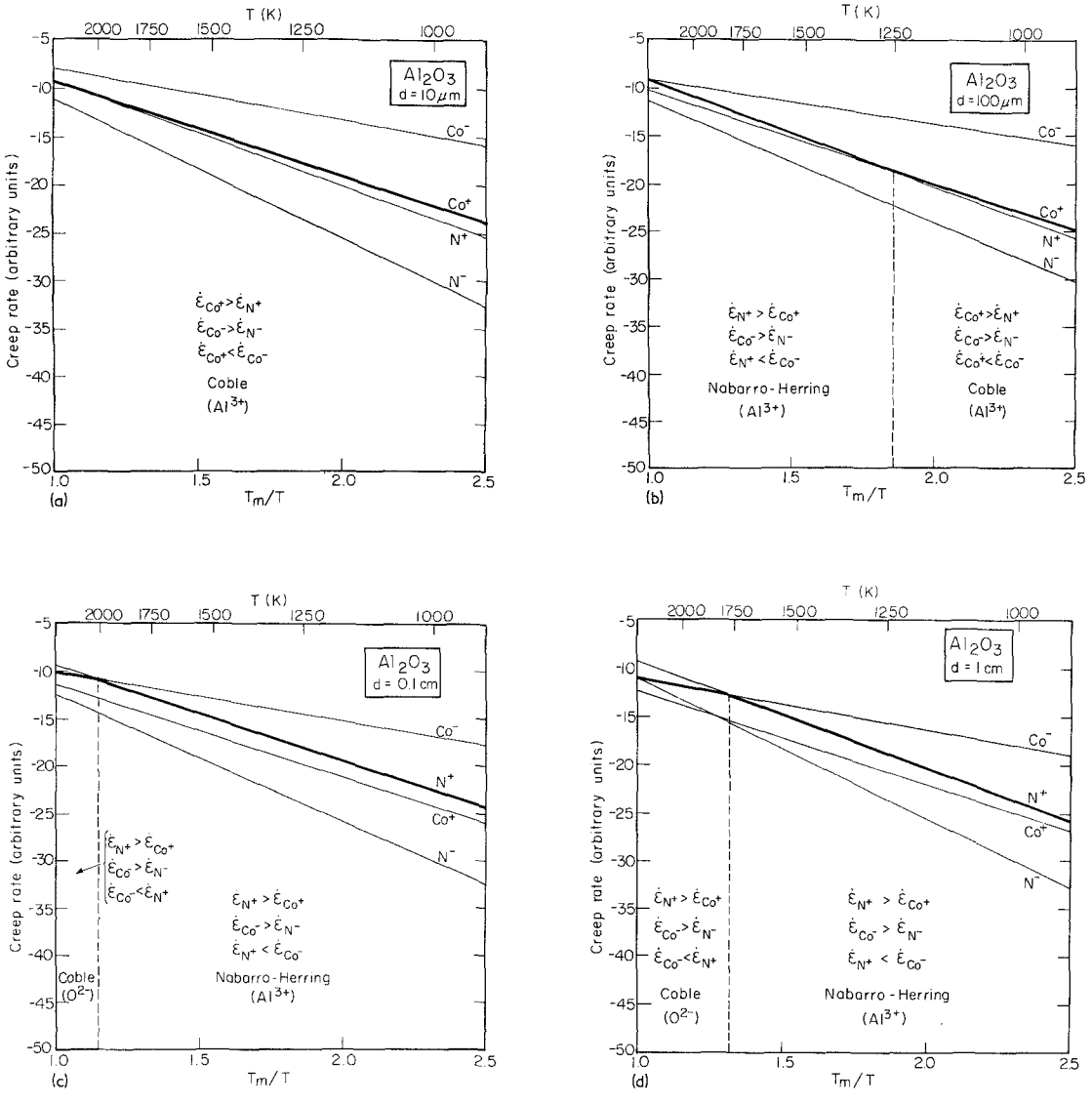

Figure 2 Logarithmic creep rate versus the reciprocal of homologous temperature for polycrystalline Al_2O_3 having grain sizes of (a) 10 μm, (b) 100 μm, (c) 0.1 cm, (d) 1 cm. The calculations indicate the rate-controlling process.

creep at a temperature of ~ 1250 K. Because the slopes of the lines for $\dot{\epsilon}^+_{Co}$ and $\dot{\epsilon}^+_N$ are very similar it is difficult to use Fig. 2a to derive the exact temperature of transition from cation-controlled Coble creep to cation-controlled Nabarro–Herring creep. As will be demonstrated by the use of a deformation mechanism map, the transition occurs at a temperature which is slightly below the melting point for a grain size of 10 μm.

The form of the transition shown in Fig. 2b, from Coble creep at lower temperatures to Nabarro–Herring creep at higher temperatures, is in conformity with the standard behaviour in monatomic systems, whereas for a grain size of 0.1 cm, given in Fig. 2c, cation-controlled Nabarro–Herring creep dominates over most of the temperature range but there is a transition to anion-controlled Coble creep at temperatures above ~ 2000 K. The transition from Nabarro–Herring creep at lower temperatures to Coble creep at higher temperatures is also evident for a grain size of 1 cm, as shown in Fig. 2d, but, because of the additional $1/d$ term in Equation 9 which reduces the magnitude of $\dot{\epsilon}^-_{Co}$ at larger grain sizes, the transition temperature is then reduced to ~ 1800 K.

4. A deformation mechanism map for diffusion creep in Al_2O_3

4.1. Construction of the map

The equations for diffusion creep in a ceramic material are given in Table I. An important similarity between these processes is that each is linearly related to the applied stress. The two variables in the constitutive relationships are grain size, because of the additional $1/d$ term in the Coble equations, and temperature, which enters as an exponential term through the diffusion coefficient.

As discussed elsewhere [31], when several mechanisms have the same dependence on stress, such as Newtonian viscous processes in diffusion creep, it is possible to construct a simple deformation mechanism map which is independent of the selected stress level. This is achieved by plotting the normalized grain size, d/b, as a function of the reciprocal of the homologous temperature, T_m/T, from $0.4\,T_m$ to the melting point. A reciprocal temperature relationship is used so that the boundaries separating the various fields in grain size–temperature space appear on the map as straight lines.

Following the construction procedure described elsewhere [31], Fig. 3 shows the map obtained for Al_2O_3 using Equations 6 to 9. The lines in Fig. 3 represent the boundaries between fields within which a single diffusion creep mechanism dominates the behaviour. The scale of normalized grain size, d/b, is from 2×10^3 to 2×10^8, which corresponds to grain sizes from $\sim 1\,\mu m$ to 9.5 cm.

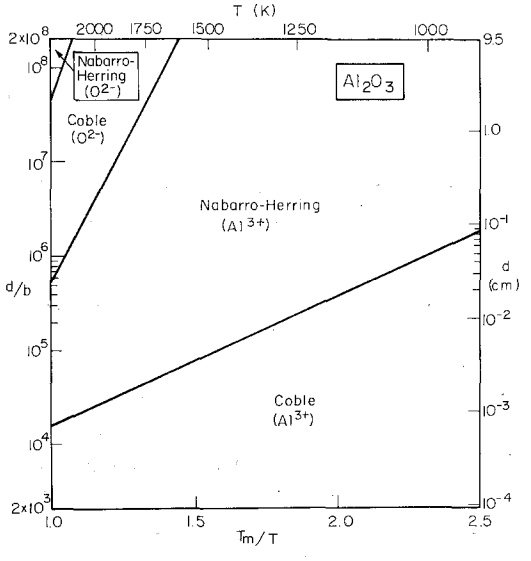

Figure 3 Deformation mechanism map of normalized grain size versus the reciprocal of homologous temperature for the four diffusion creep processes in Al_2O_3. This map is independent of the selected stress level.

As indicated on the map, cation-controlled Coble creep is the dominant mechanism of diffusion creep at low temperatures and small grain sizes. As the temperature and grain size are increased, there is a transition to cation-controlled Nabarro–Herring creep, anion-controlled Coble creep, and, at very large grain sizes ($d \geqslant 2$ cm) and temperatures very near to the melting point ($T \geqslant 2300$ K), anion-controlled Nabarro–Herring creep.

The map shown in Fig. 3 is independent of the stress level. Provided the stress is sufficiently low in a real situation that the behaviour is controlled by diffusion creep rather than a dislocation mechanism, the rate-controlling process may be obtained directly from the map. Maps of the type shown in Fig. 3 represent a powerful tool in the evaluation of creep behaviour*. For example, for polycrystalline samples of Al_2O_3 having grain sizes in the range from 100 to 500 μm tested at temperatures from 1500 to 2000 K, the map shows that the rate-controlling process in the diffusion creep regime is Nabarro–Herring creep controlled by diffusion of the Al^{3+} ions. Conversely, if the same samples are tested at 1000 K, the rate-controlling process is Coble creep controlled by diffusion of the Al^{3+} ions.

4.2. Insertion of constant strain rate contours

The field boundaries in Fig. 3 trace out the loci of points where the two adjacent processes have equal strain rates. It is a simple procedure to insert contours of constant strain rate on to the map for any selected stress level, since the field boundaries remain fixed in grain size–temperature space.

Two examples are shown in Fig. 4, corresponding to values of normalized stress, σ/G, of 10^{-6} and 10^{-3}, respectively. Fig. 4a shows the contours for two strain rates of particular interest, 10^{-10} and 10^{-9} sec^{-1}, corresponding to an upper limiting strain rate for many structural design purposes and a lower limiting strain rate for most laboratory experiments, respectively. For simplicity, the contours are shown as straight lines up to the field boundaries, although in practice this introduces a slight error because the contours are

*The completion of the map through the incorporation of dislocation creep is described in Section 5.

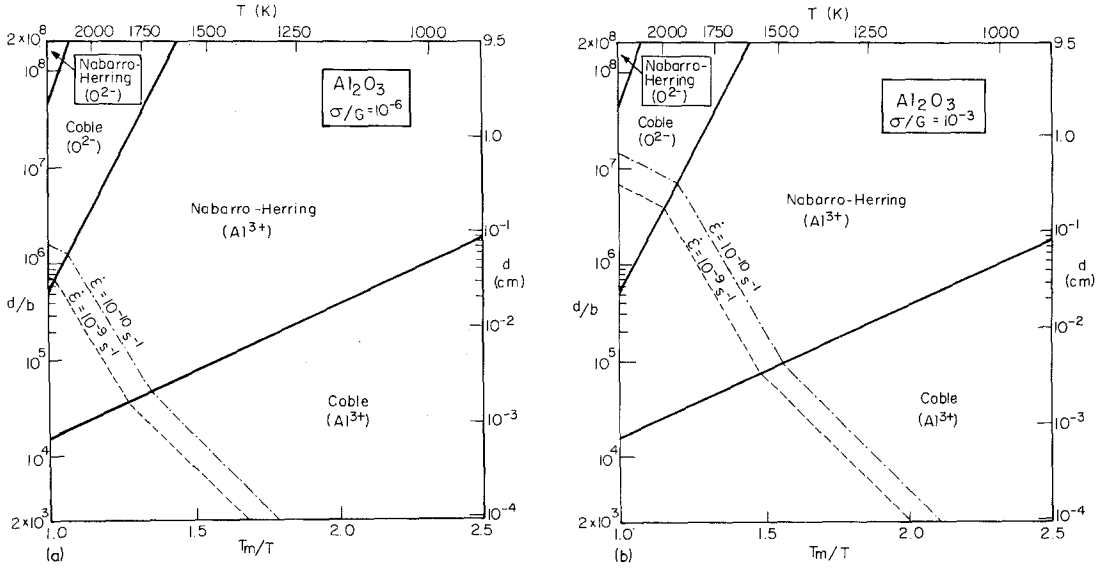

Figure 4 Deformation mechanism map of normalized grain size versus the reciprocal of homologous temperature for the four diffusion creep processes in Al_2O_3, showing constant strain rate contours for normalized stresses of (a) 10^{-6}, (b) 10^{-3}.

curved in the immediate vicinity of the boundaries. The contours shown in Fig. 4 were inserted by a simple procedure described elsewhere [31]. If required, the exact positions of the contours may be calculated over the entire map by solving Equation 4 with a computer, thereby including the curvature in the vicinity of the field boundaries. In view of the rather large uncertainties associated with the diffusion coefficients for Al_2O_3, as given by Equations 10 to 13, and with the corresponding uncertainties in the diffusion coefficients for other ionic compounds, it seems reasonable not to include this additional refinement at the present time. As indicated by a comparison of Figs. 4a and b, the effect of an increase in stress level is to displace the contours to larger grain sizes.

5. Deformation mechanism maps for Al_2O_3 including dislocation creep

The map developed for Al_2O_3 in Fig. 3 relates specifically to the four Newtonian viscous processes of diffusion creep. The map is therefore incomplete for use at all stress levels during high temperature creep, because Al_2O_3 may also deform by a dislocation process.

The steady-state creep rate for the dislocation mechanism is given by

$$\dot{\epsilon}_c = A_c\left(\frac{Gb}{kT}\right)\left(\frac{\sigma}{G}\right)^n D_l \qquad (14)$$

where D_l is the lattice diffusion coefficient for the slower moving ion (D_l^- for Al_2O_3), and A_c and n are constants. Based on the available creep data for polycrystalline Al_2O_3, it is estimated that $n = 3$ and $A_c = 4$ [24]. The precise nature of the dislocation process is not known at the present time, and the mechanism is henceforth designated dislocation creep.

It is evident from Equation 14 that dislocation creep is independent of grain size but varies with the applied stress raised to the third power. This means that the mechanism is primarily important at large grain sizes, and also that it increases in importance as the stress level is raised. This effect is demonstrated by the deformation mechanism maps in Fig. 5 for normalized stresses of 10^{-6}, 10^{-4}, and 10^{-3}, respectively. The field boundaries for the diffusion creep processes remain in identical positions at all stress levels, but dislocation creep gradually extends to smaller grain sizes and lower temperatures as the stress is increased. The constant strain rate contours are again shown in Fig. 5, to permit a direct comparison with Fig. 4.

An examination of Fig. 5a shows that it is experimentally impossible to observe Nabarro–Herring creep controlled by anion diffusion in pure Al_2O_3. At $\sigma/G = 10^{-6}$, the field for anion-controlled Nabarro–Herring creep is excluded by the dislocation creep process. This latter process may be removed from the map by decreasing the value of σ/G, but the strain rate contours are then

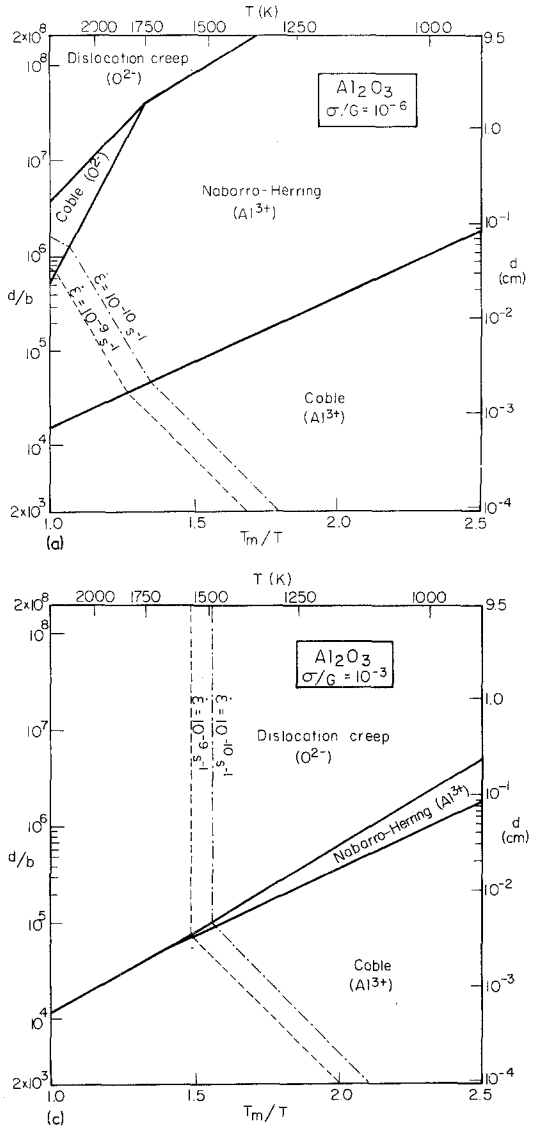

Figure 5 Deformation mechanism map of normalized grain size versus the reciprocal of homologous temperature for diffusion creep and dislocation creep in Al_2O_3, for normalized stresses of (a) 10^{-6}, (b) 10^{-4}, (c) 10^{-3}.

displaced to smaller grain sizes. It is apparent that the strain rates associated with anion-controlled Nabarro–Herring creep are too small to measure in laboratory experiments.

It is also evident from Fig. 5a that it is difficult, but not impossible, to experimentally observe anion-controlled Coble creep in pure Al_2O_3, since the required temperatures are very high and the resultant strain rates are near to the lower limit of convenient laboratory detection.

A comparison of Figs. 5b and c reveals two criteria which must be fulfilled in order to observe cation-controlled Nabarro–Herring creep in laboratory experiments on pure Al_2O_3: (1) the normalized stress level must be less than $\sim 10^{-3}$, since at higher stresses the cation-controlled Nabarro–Herring field is effectively excluded by the dislocation creep process; (2) the testing temperature must be above ~ 1600 K, since at lower temperatures the strain rates are too slow for convenient measurement at the required stress levels.

6. Discussion

Deformation mechanism maps provide a very useful method of displaying mechanical data, especially for conditions of high temperature creep. The maps developed in this report differ in two important respects from those previously published for ceramic materials. First, the maps recognize the presence of two atomic species in ceramics, by incorporating ambipolar diffusion to give four constitutive relationships for diffusion creep. Second, the maps are presented in a new format which is particularly suited for ionic compounds at high temperatures. By plotting normalized grain size, d/b, against the reciprocal of homologous temperature, T_m/T, for pure Al_2O_3, it is demonstrated that the four alternative processes for diffusion creep may be represented on a simple map which is independent of the selected stress level.

Although simple to construct, maps of this type provide very useful information in the planning and interpretation of creep experiments.

Since each of the four diffusion creep processes is only dominant over a limited range of temperature and grain size, the map may be used to determine the rate-controlling mechanism for diffusion creep under any selected experimental conditions. By superimposing on to the map the best available data for dislocation creep, estimates may be made of the highest permissible stress and the lowest feasible temperature for experimental observation of any of the diffusion creep processes (for example, from Fig. 5c, $\sigma/G < 10^{-3}$ and $T > 1600\,K$ for cation-controlled Nabarro–Herring creep in Al_2O_3).

It must be emphasized that all deformation mechanism maps are necessarily only accurate within the accuracy of the constitutive relationships, and the values for the various diffusion coefficients, used in their construction. This is clearly important in ceramic materials, where there is often rather limited information on the appropriate values for $\delta^+D^+_{gb}$ and $\delta^-D^-_{gb}$. A map of the type developed for diffusion creep processes in Al_2O_3 (Fig. 3) represents a best estimate based on the diffusion data available at the present time. Any future improvements in the experimental measurements of the diffusion coefficients will, of course, lead to modifications and improvements in the map.

Finally, it should be noted that no attempt has been made in this report to examine the effect of doping on the positions of the field boundaries in the maps. Since selective doping may significantly affect the values of the diffusion coefficients, this leads to the possibility of using doping to modify the basic deformation mechanism map for the diffusion creep processes.

7. Summary and conclusions

(1) In an ionic compound, ambipolar diffusion may take place so that there is simultaneous mass transport of the anions and cations along parallel, but different, diffusion paths. This gives rise to four distinct types of diffusion creep, depending on whether Nabarro–Herring and Coble creep is controlled by the anions or cations, respectively.

(2) Ambipolar diffusion was incorporated in a deformation mechanism map for diffusion creep in pure Al_2O_3, using a new form of map which is independent of the selected stress level. This map indicates the rate-controlling mechanism for diffusion creep under any selected experimental conditions.

(3) By superimposing dislocation creep on to the map, it was demonstrated that (a) it is experimentally impossible to observe anion-controlled Nabarro–Herring creep in pure polycrystalline Al_2O_3 in the laboratory, and (b) it is difficult to observe anion-controlled Coble creep in Al_2O_3 because the required temperatures are very high and the resultant strain rates are near to the lower limit for laboratory detection.

Acknowledgement

This work was supported by the United States Energy Research and Development Administration under Contract E(04-3)-113 PA-26.

References

1. M. F. ASHBY, *Acta Met.* **20** (1972) 887.
2. A. G. GUY, "Essentials of Materials Science" (McGraw–Hill, New York, 1976) p. 324.
3. R. W. HERTZBERG, "Deformation and Fracture Mechanics of Engineering Materials" (John Wiley, New York, 1976) p. 156.
4. W. D. KINGERY, H. K. BOWEN and D. R. UHLMANN, "Introduction to Ceramics," 2nd edition (John Wiley, New York, 1976) p. 745.
5. B. ILSCHNER, "Hochtemperatur-Plastizität", Reine und angewandte Metallkunde in Einzeldarstallungen, Vol. 23 (Springer-Verlag, Berlin, 1973) p. 258.
6. J. GITTUS, "Creep, Viscoelasticity and Creep Fracture in Solids" (John Wiley, New York, 1975) p. 274
7. J. -P. POIRIER, "Plasticité à Haute Température des Solides Cristallins" (Eyrolles, Paris, 1976) p. 156.
8. A. NICOLAS and J. -P. POIRIER, "Crystalline Plasticity and Solid State Flow in Metamorphic Rocks" (John Wiley, London, 1976) p. 403.
9. J. WEERTMAN and J. R. WEERTMAN, "Physical Metallurgy," edited by R. W. Cahn (North–Holland, Amsterdam, 1965) p. 793.
10. J. WEERTMAN, *Trans. ASM* **61** (1968) 681.
11. F. A. MOHAMED and T. G. LANGDON, *Met. Trans.* **5** (1974) 2339.
12. P. A. URICK and M. R. NOTIS, *J. Amer. Ceram. Soc.* **56** (1973) 570.
13. M. R. NOTIS, *Powder Met. Intl.* **6** (1974) 82.
14. M. R. NOTIS, R. H. SMOAK and V. KRISHNAMACHARI, *Mater. Sci. Res.* **10** (1975) 493.
15. R. L. STOCKER and M. F. ASHBY, *Rev. Geophys. Space Phys.* **11** (1973) 391.
16. J. WEERTMAN and J. R. WEERTMAN, *Ann. Rev. Earth and Planetary Sci.* **3** (1975) 293.
17. M. F. ASHBY, *J. Geol. Soc.* **132** (1976) 558.
18. M. R. NOTIS, *J. Amer. Ceram. Soc.* **57** (1974) 271.
19. B. K. ATKINSON, *Earth and Planetary Sci. Let.* **29** (1976) 210.
20. V. KRISHNAMACHARI and M. R. NOTIS, *Mater. Sci. Eng.* **27** (1977) 83.
21. R. N. SINGH, *J. Nuclear Mater.* **64** (1977) 167.

22. J. T. A. ROBERTS and J. C. VOGLEWEDE, *J. Amer. Ceram. Soc.* **56** (1973) 472.
23. M. F. ASHBY and H. J. FROST, "Constitutive Equations in Plasticity," edited by A. S. Argon (MIT Press, Cambridge, Mass., 1975) p. 117.
24. T. G. LANGDON and F. A. MOHAMED, *J. Mater. Sci.* **11** (1976) 317.
25. F. R. N. NABARRO, "Report of a Conference on Strength of Solids" (The Physical Society, London, 1948) p. 75.
26. C. HERRING, *J. Appl. Phys.* **21** (1950) 437.
27. R. L. COBLE, *ibid* **34** (1963) 1679.
28. R. S. GORDON, *J. Amer. Ceram. Soc.* **56** (1973) 147.
29. R. S. GORDON and J. D. HODGE, *J. Mater. Sci.* **10** (1975) 200.
30. R. S. GORDON, "Mass Transport Phenomena in Ceramics," edited by A. R. Cooper and A. H. Heuer (Plenum Press, New York, 1975) p. 445.
31. T. G. LANGDON and F. A. MOHAMED, *Mater. Sci. Eng.* **32** (1978) 103.
32. A. G. EVANS and T. G. LANGDON, *Prog. Mater. Sci.* **21** (1976) 171.
33. A. E. PALADINO and W. D. KINGERY, *J. Chem. Phys.* **37** (1962) 957.
34. R. M. CANNON and R. L. COBLE, "Deformation of Ceramic Materials," edited by R. C. Bradt and R. E. Tressler (Plenum Press, New York, 1975) p. 61.
35. Y. OISHI and W. D. KINGERY, *J. Chem. Phys.* **33** (1960) 480.

Received 16 March and accepted 28 April 1977.